Hinkkanen, Marko; Tuovinen, Toni; Harnefors, Lennart; Luomi, Jorma

A combined position and stator-resistance observer for salient PMSM drives

Published in:
IEEE Transactions on Power Electronics

DOI:
10.1109/TPEL.2011.2118232

Published: 01/01/2012

Document Version
Peer reviewed version

Please cite the original version:
Hinkkanen, M., Tuovinen, T., Harnefors, L., & Luomi, J. (2012). A combined position and stator-resistance observer for salient PMSM drives: design and stability analysis. *IEEE Transactions on Power Electronics*, *27*(2), 601-609. https://doi.org/10.1109/TPEL.2011.2118232

A Combined Position and Stator-Resistance Observer for Salient PMSM Drives: Design and Stability Analysis

Marko Hinkkanen, *Member, IEEE,* Toni Tuovinen, Lennart Harnefors, *Senior Member, IEEE,* and Jorma Luomi, *Member, IEEE*

***Abstract*—A reduced-order position observer with stator-resistance adaptation is proposed for motion-sensorless permanent-magnet synchronous motor drives. A general analytical solution for the stabilizing observer gain and stability conditions for the stator-resistance adaptation are derived. Under these conditions, the local stability of the position and stator-resistance estimation is guaranteed at every operating point except the zero frequency, if other motor parameters are known. Furthermore, the effect of inaccurate model parameters on the local stability of the position estimation is studied, and an observer gain design that makes the observer robust is proposed. The proposed observer is experimentally tested using a 2.2-kW motor drive; stable operation at very low speeds under different loading conditions is demonstrated.**

***Index Terms*—Interior magnet, observer, salient, sensorless, stability conditions, stator-resistance estimation.**

I. Introduction

Sensorless control of permanent-magnet synchronous motors (PMSMs) is today a mature topic, in research as well as in application. The benefits of not having to rely on position sensors, i.e., lower cost and volume, less cabling, and increased reliability, are well known.

For salient PMSMs, signal-injection-based methods [1], [2], [3] can be used. Such methods allow a very accurate position estimate to be obtained at all speeds, including standstill. Their drawbacks include increased acoustic noise, losses, and vibration. Consequently, it is useful to, once out of the very-low-speed region, make a smooth transition to a back-electromotive-force (EMF)-based method [4]–[9]. To facilitate this transition at as low a speed as possible, it is vital to use a back-EMF-based method by which an asymptotically stable system is obtained for all speeds but standstill.[1]

The stator resistance is the by far most sensitive parameter at low speeds; an inaccurate model stator resistance will often result in a large position error [10], [11], [12], and possibly even instability. Among the many publications on back-EMF-based methods for PMSMs [8], [10]–[30], only a few have proposed circumvention of this problem. Most of these proposed solutions involve on-line resistance estimation [19], [21], [23]—in effect resulting in a combined position and stator-resistance observer—whereas [11] proposes usage of the instantaneous reactive power.

Designing a combined position and stator-resistance observer with the desired property, i.e., asymptotic stability for all speeds but standstill, requires careful analysis. To the best knowledge of the authors, this has so far only been achieved for nonsalient PMSMs [21], [23]. The fundamental contribution of this paper is the design of such an observer for salient PMSMs. After a review of the model considered in Section II, the main results of the paper are presented in Section III. These are as follows:

1) A reduced-order position observer for salient PMSM drives is proposed.
2) Analytical stability conditions for this observer are derived and formulated as a general stabilizing gain. This simplifies the tuning procedure.
3) The effects of the free design parameters of the stabilizing gain on the robustness of the position estimation are analyzed, and a robust gain design is proposed.
4) The observer is thereafter augmented with the stator-resistance adaptation, and analytical stability conditions are derived for the augmented observer.

The proposed design is comparatively simple, and it results in a robust and well-damped closed-loop system. Though we for brevity do not address this explicitly, the observer can easily be augmented with a signal-injection method in the immediate region of zero speed, for example in a fashion similar to [5], [7]. Performance of the proposed observer design is evaluated in Section IV using laboratory experiments with a 2.2-kW PMSM drive.

II. PMSM Model

Real space vectors will be used throughout the paper. For example, the stator-current vector is $\boldsymbol{i}_\mathrm{s} = [i_\mathrm{d}, i_\mathrm{q}]^\mathrm{T}$, where i_d and i_q are the components of the vector and the matrix transpose is marked with the superscript T. The identity matrix and the orthogonal rotation matrix are defined as

$$\mathbf{I} = \begin{bmatrix} 1 & 0 \\ 0 & 1 \end{bmatrix}, \quad \mathbf{J} = \begin{bmatrix} 0 & -1 \\ 1 & 0 \end{bmatrix}$$

respectively.[2]

The preliminary version of this paper was presented at the IEEE International Symposium on Industrial Electronics (ISIE), Bari, Italy, July 4–7, 2010.

[1]Because the back EMF vanishes at zero rotor speed, a back-EMF-based estimator by necessity becomes "blind," and as a consequence marginally stable, at standstill.

[2]The notation is very similar to that obtained for complex space vectors: the rotation matrix $\mathbf{J}$ corresponds to the imaginary unit j and the coordinate transformation matrices can be expressed using matrix exponentials, i.e. $\mathrm{e}^{\vartheta\mathbf{J}} = \cos\vartheta\mathbf{I} + \sin\vartheta\mathbf{J}$.

The electrical angular position of the permanent-magnet flux is denoted by ϑ_m. The position depends on the electrical angular rotor speed ω_m according to

$$\frac{\mathrm{d}\vartheta_\mathrm{m}}{\mathrm{d}t} = \omega_\mathrm{m} \tag{1}$$

To simplify the analysis in the following sections, the machine model will be expressed in the *estimated* rotor reference frame, whose d axis is aligned at $\hat{\vartheta}_\mathrm{m}$ with respect to the stator reference frame. The inductance matrix and the permanent-magnet-flux vector are

$$\boldsymbol{L} = \mathrm{e}^{-\tilde{\vartheta}_\mathrm{m}\mathbf{J}} \begin{bmatrix} L_\mathrm{d} & 0 \\ 0 & L_\mathrm{q} \end{bmatrix} \mathrm{e}^{\tilde{\vartheta}_\mathrm{m}\mathbf{J}}, \quad \boldsymbol{\psi}_\mathrm{pm} = \mathrm{e}^{-\tilde{\vartheta}_\mathrm{m}\mathbf{J}} \begin{bmatrix} \psi_\mathrm{pm} \\ 0 \end{bmatrix} \tag{2}$$

respectively, where $\tilde{\vartheta}_\mathrm{m} = \hat{\vartheta}_\mathrm{m} - \vartheta_\mathrm{m}$ is the estimation error in the rotor position, L_d the direct-axis inductance, L_q the quadrature-axis inductance, and ψ_pm the permanent-magnet flux. The voltage equation is

$$\frac{\mathrm{d}\boldsymbol{\psi}_\mathrm{s}}{\mathrm{d}t} = \boldsymbol{u}_\mathrm{s} - R_\mathrm{s}\boldsymbol{i}_\mathrm{s} - \hat{\omega}_\mathrm{m}\mathbf{J}\boldsymbol{\psi}_\mathrm{s} \tag{3a}$$

where $\boldsymbol{\psi}_\mathrm{s}$ is the stator-flux vector, $\boldsymbol{u}_\mathrm{s}$ the stator-voltage vector, R_s the stator resistance, and $\hat{\omega}_\mathrm{m} = \mathrm{d}\hat{\vartheta}_\mathrm{m}/\mathrm{d}t$ is the angular speed of the coordinate system. The stator current is a nonlinear function

$$\boldsymbol{i}_\mathrm{s} = \boldsymbol{L}^{-1}(\boldsymbol{\psi}_\mathrm{s} - \boldsymbol{\psi}_\mathrm{pm}) \tag{3b}$$

of the stator-flux vector and the position error $\tilde{\vartheta}_\mathrm{m}$.

III. Rotor-Position Observer

A typical rotor-oriented control system is depicted in Fig. 1. The rotor-position observer in estimated rotor coordinates is considered. The current reference $\boldsymbol{i}_\mathrm{s,ref}$ is used for controlling the electromagnetic torque (and the flux linkage). The stator currents and the dc-link voltage u_dc are measured, and the reference voltage $\boldsymbol{u}_\mathrm{s,ref}$ obtained from the current controller is used for the observer. In the following analysis, it will be assumed that the effect of the inverter nonlinearities are perfectly compensated, i.e. $\boldsymbol{u}_\mathrm{s} = \boldsymbol{u}_\mathrm{s,ref}$. Estimates and model parameters will be marked by hats.

Since the rotor-position estimation error is unknown, the model inductance matrix and the model permanent-magnet-flux vector are

$$\hat{\boldsymbol{L}} = \begin{bmatrix} \hat{L}_\mathrm{d} & 0 \\ 0 & \hat{L}_\mathrm{q} \end{bmatrix}, \quad \hat{\boldsymbol{\psi}}_\mathrm{pm} = \begin{bmatrix} \hat{\psi}_\mathrm{pm} \\ 0 \end{bmatrix} \tag{4}$$

respectively. The actual inductance matrix $\boldsymbol{L}$ and the permanent-magnet flux vector $\boldsymbol{\psi}_\mathrm{pm}$ given in (2) are not generally equal to $\hat{\boldsymbol{L}}$ and $\hat{\boldsymbol{\psi}}_\mathrm{pm}$, respectively; the position-estimation error $\tilde{\vartheta}_\mathrm{m}$ appearing in (2) can be nonzero in transient states, even if accurate model parameters in (4) were assumed.

A. Speed-Adaptive Observer

A conventional method for estimating the rotor position is to apply an observer [8], [16]

$$\frac{\mathrm{d}\hat{\boldsymbol{\psi}}_\mathrm{s}}{\mathrm{d}t} = \boldsymbol{u}_\mathrm{s} - \hat{R}_\mathrm{s}\boldsymbol{i}_\mathrm{s} - \hat{\omega}_\mathrm{m}\mathbf{J}\hat{\boldsymbol{\psi}}_\mathrm{s} + \boldsymbol{K}(\hat{\boldsymbol{i}}_\mathrm{s} - \boldsymbol{i}_\mathrm{s}) \tag{5a}$$

$$\hat{\boldsymbol{i}}_\mathrm{s} = \hat{\boldsymbol{L}}^{-1}(\hat{\boldsymbol{\psi}}_\mathrm{s} - \hat{\boldsymbol{\psi}}_\mathrm{pm}) \tag{5b}$$

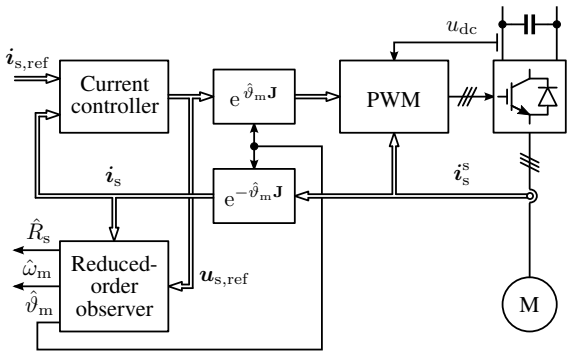

Fig. 1. Motion-sensorless rotor-oriented controller. The observer is implemented in estimated rotor coordinates. The superscript s refers to stator coordinates. The pulse-width modulator (PWM) applies the current feedback for compensation of inverter nonlinearities.

where $\hat{\boldsymbol{\psi}}_\mathrm{s} = [\hat{\psi}_\mathrm{d}, \hat{\psi}_\mathrm{q}]^\mathrm{T}$ and $\boldsymbol{K}$ is a 2×2 observer gain matrix. The dynamics of the rotor-position estimate are described by

$$\frac{\mathrm{d}\hat{\vartheta}_\mathrm{m}}{\mathrm{d}t} = \hat{\omega}_\mathrm{m} \tag{6}$$

In order to estimate the rotor speed, the observer is augmented with a speed-adaptation law. Typically, the estimation error $\hat{i}_\mathrm{q} - i_\mathrm{q}$ is fed to the PI mechanism whose output is the speed estimate

$$\hat{\omega}_\mathrm{m} = k_\mathrm{p}(\hat{i}_\mathrm{q} - i_\mathrm{q}) + k_\mathrm{i}\int(\hat{i}_\mathrm{q} - i_\mathrm{q})\mathrm{d}t \tag{7}$$

where k_p and k_i are adaptation gains. The speed-adaptive observer consisting of (5), (6), and (7) is of the fourth order, and there are four parameters to tune (assuming that $\boldsymbol{K}$ is skew-symmetric). This observer will be used as a starting point in the following.

B. Proposed Reduced-Order Observer

1) Observer Structure: The observer order can be reduced by estimating only the d component $\hat{\psi}_\mathrm{d}$ while the q component is evaluated based on the measured current. The stator-flux estimate is redefined as

$$\hat{\boldsymbol{\psi}}_\mathrm{s} = \begin{bmatrix} \hat{\psi}_\mathrm{d} \\ \hat{\psi}_\mathrm{q} \end{bmatrix} = \begin{bmatrix} \hat{L}_\mathrm{d}\hat{i}_\mathrm{d} + \hat{\psi}_\mathrm{pm} \\ \hat{L}_\mathrm{q} i_\mathrm{q} \end{bmatrix} \tag{8}$$

Since the q component of the current-estimation error is not available, the observer gain reduces to

$$\boldsymbol{K} = \begin{bmatrix} \hat{L}_\mathrm{d}k_1 & 0 \\ \hat{L}_\mathrm{d}k_2 & 0 \end{bmatrix} \tag{9}$$

where the two gain components k_1 and k_2 are scaled with $\hat{L}_\mathrm{d}$ for convenience. Using the definitions (8) and (9) in (5), the componentwise presentation of the proposed reduced-order observer becomes

$$\frac{\mathrm{d}\hat{\psi}_\mathrm{d}}{\mathrm{d}t} = u_\mathrm{d} - \hat{R}_\mathrm{s}i_\mathrm{d} + \hat{\omega}_\mathrm{m}\hat{L}_\mathrm{q}i_\mathrm{q} + k_1(\hat{\psi}_\mathrm{d} - \hat{\psi}_\mathrm{pm} - \hat{L}_\mathrm{d}i_\mathrm{d}) \tag{10a}$$

$$\frac{\mathrm{d}\hat{\vartheta}_\mathrm{m}}{\mathrm{d}t} = \frac{u_\mathrm{q} - \hat{R}_\mathrm{s}i_\mathrm{q} - \hat{L}_\mathrm{q}\frac{\mathrm{d}i_\mathrm{q}}{\mathrm{d}t} + k_2(\hat{\psi}_\mathrm{d} - \hat{\psi}_\mathrm{pm} - \hat{L}_\mathrm{d}i_\mathrm{d})}{\hat{\psi}_\mathrm{d}} = \hat{\omega}_\mathrm{m} \tag{10b}$$

It can be seen that the rotor speed estimate is obtained directly from (10b). The speed-adaptation law is avoided and the implementation becomes easier. The proposed observer is of the second order and there are only two gains. The digital implementation of (10) can be formed as

$$\hat{\omega}_{\mathrm{m}}^{k} = \frac{1}{\hat{\psi}_{\mathrm{d}}^{k}}\Bigg[u_{\mathrm{q}}^{k} - \hat{R}_{\mathrm{s}} i_{\mathrm{q}}^{k} - \hat{L}_{\mathrm{q}} \frac{i_{\mathrm{q}}^{k} - i_{\mathrm{q}}^{k-1}}{T_{\mathrm{s}}} + k_2(\hat{\psi}_{\mathrm{d}}^{k} - \hat{\psi}_{\mathrm{pm}} - \hat{L}_{\mathrm{d}} i_{\mathrm{d}}^{k})\Bigg] \tag{11a}$$

$$\hat{\psi}_{\mathrm{d}}^{k+1} = \hat{\psi}_{\mathrm{d}}^{k} + T_{\mathrm{s}}\big[u_{\mathrm{d}}^{k} - \hat{R}_{\mathrm{s}} i_{\mathrm{d}}^{k} + \hat{\omega}_{\mathrm{m}}^{k} \hat{L}_{\mathrm{q}} i_{\mathrm{q}}^{k} + k_1(\hat{\psi}_{\mathrm{d}}^{k} - \hat{\psi}_{\mathrm{pm}} - \hat{L}_{\mathrm{d}} i_{\mathrm{d}}^{k})\big] \tag{11b}$$

$$\hat{\vartheta}_{\mathrm{m}}^{k+1} = \hat{\vartheta}_{\mathrm{m}}^{k} + T_{\mathrm{s}} \hat{\omega}_{\mathrm{m}}^{k} \tag{11c}$$

where T_{s} is the sampling period and k is the sampling index representing the time instant $t = kT_{\mathrm{s}}$.

2) Nonlinear Estimation-Error Dynamics: From (3) and (5), the nonlinear dynamics of the estimation error become

$$\frac{\mathrm{d}\tilde{\boldsymbol{\psi}}_{\mathrm{s}}}{\mathrm{d}t} = (\boldsymbol{K}\hat{\boldsymbol{L}}^{-1} - \hat{\omega}_{\mathrm{m}}\mathbf{J})\tilde{\boldsymbol{\psi}}_{\mathrm{s}} - \boldsymbol{K}\hat{\boldsymbol{L}}^{-1}\tilde{\boldsymbol{\psi}}_{\mathrm{pm}} + \boldsymbol{K}(\hat{\boldsymbol{L}}^{-1}\boldsymbol{L} - \mathbf{I})\boldsymbol{i}_{\mathrm{s}} - \tilde{R}_{\mathrm{s}}\boldsymbol{i}_{\mathrm{s}} \tag{12a}$$

$$\frac{\mathrm{d}\tilde{\vartheta}_{\mathrm{m}}}{\mathrm{d}t} = \tilde{\omega}_{\mathrm{m}} \tag{12b}$$

where $\tilde{\boldsymbol{\psi}}_{\mathrm{s}} = \hat{\boldsymbol{\psi}}_{\mathrm{s}} - \boldsymbol{\psi}_{\mathrm{s}}$, $\tilde{\boldsymbol{\psi}}_{\mathrm{pm}} = \hat{\boldsymbol{\psi}}_{\mathrm{pm}} - \boldsymbol{\psi}_{\mathrm{pm}}$, $\tilde{R}_{\mathrm{s}} = \hat{R}_{\mathrm{s}} - R_{\mathrm{s}}$, and $\tilde{\omega}_{\mathrm{m}} = \hat{\omega}_{\mathrm{m}} - \omega_{\mathrm{m}}$. The estimation-error dynamics of the proposed observer (10) are described by (12) with the condition given in (8) and the observer gain given in (9).

3) Stabilizing Observer Gain: The gains k_1 and k_2 in (10) determine the stability (and other properties) of the observer. To avoid forbiddingly complicated equations, which would prevent analytical results from being derived, accurate model parameters $\hat{R}_{\mathrm{s}}$, $\hat{L}_{\mathrm{d}}$, $\hat{L}_{\mathrm{q}}$, and $\hat{\psi}_{\mathrm{pm}}$ are first assumed. As shown in Appendix A, the closed-loop system consisting of (3) and (10) is locally stable in every operating point if (and only if) the gains are given by[3]

$$k_1 = -\frac{b + \beta(c/\hat{\omega}_{\mathrm{m}} - \hat{\omega}_{\mathrm{m}})}{\beta^2 + 1}, \quad k_2 = \frac{\beta b - c/\hat{\omega}_{\mathrm{m}} + \hat{\omega}_{\mathrm{m}}}{\beta^2 + 1} \tag{13}$$

where the design parameters $b > 0$ and $c > 0$ may depend on the operating point and

$$\beta = \frac{(\hat{L}_{\mathrm{d}} - \hat{L}_{\mathrm{q}}) i_{\mathrm{q}}}{\hat{\psi}_{\mathrm{pm}} + (\hat{L}_{\mathrm{d}} - \hat{L}_{\mathrm{q}}) i_{\mathrm{d}}} \tag{14}$$

As two special cases, (14) reduces to $\beta = 0$ for non-salient PMSMs and $\beta = i_{\mathrm{q}}/i_{\mathrm{d}}$ for synchronous reluctance machines.

The observer gain design problem is reduced to the selection of the two positive parameters b and c, which are actually the coefficients of the characteristic polynomial of the linearized closed-loop system, cf. Appendix A. Hence, (13) can be used to place the poles of the linearized closed-loop system arbitrarily.

[3]For $\hat{\omega}_{\mathrm{m}} = 0$, $c = 0$ has to be selected to avoid division by zero, giving only marginal stability for zero speed (i.e., there is one pole in the origin and the other pole at $-b$). A practical consequence is that the observer should be augmented with a signal-injection method if persistent zero-speed operation *under load torque* is required.

TABLE I
RATING AND PARAMETERS OF A SIX-POLE 2.2-KW PMSM

Rated speed	1500 r/min
Rated frequency	75 Hz
Rated line-to-line rms voltage	370 V
Rated rms current	4.3 A
Rated torque	14 Nm
Stator resistance R_{s}	0.067 p.u.
Direct-axis inductance L_{d}	0.35 p.u.
Quadrature-axis inductance L_{q}	0.53 p.u.
Permanent-magnet flux ψ_{pm}	0.895 p.u.

4) Robust Gain Parameters: The stability with accurate model parameters is necessary but not a sufficient design goal. The actual parameters are rarely known accurately, and in practice, they are not constant. The stator resistance and permanent-magnet flux vary with temperature during the operation of the motor. The inductances vary due to magnetic saturation. Hence, the system should be robust against parameter errors.

With parameter errors included, the stability is not guaranteed for all positive values of the design parameters b and c in (13). In the following, it is numerically studied how these design parameters should be chosen in order to reduce sensitivity to parameter errors and variations. The data of a 2.2-kW PMSM given in Table I are used. The base values for angular speed, voltage, and current are defined as $2\pi \cdot 75$ rad/s, $\sqrt{2/3} \cdot 370$ V, and $\sqrt{2} \cdot 4.3$ A, respectively. The same relative uncertainty is assumed for all four model parameters $\hat{R}_{\mathrm{s}}$, $\hat{L}_{\mathrm{d}}$, $\hat{L}_{\mathrm{q}}$, and $\hat{\psi}_{\mathrm{pm}}$. Hence, 16 different worst-case combinations, consisting of minimum and maximum values of the model parameters, can be formed. For example, if the relative uncertainty is defined to be 40%, one of the worst-case combinations is $\hat{R}_{\mathrm{s}} = 0.6R_{\mathrm{s}}$, $\hat{L}_{\mathrm{d}} = 0.6L_{\mathrm{d}}$, $\hat{L}_{\mathrm{q}} = 1.4L_{\mathrm{q}}$, and $\hat{\psi}_{\mathrm{pm}} = 1.4\psi_{\mathrm{pm}}$.

At each studied operating point, the local stability of the observer was analyzed for all 16 worst-case combinations of erroneous model parameters. First, the estimation error of the rotor position was numerically searched using (8) and (12) in steady state, i.e., $\mathrm{d}/\mathrm{d}t = 0$. If a real-valued solution for the position error (having absolute value less than 45°) was found, the small-signal stability of this operating point was analyzed by means of a linearized model obtained from (12). If the steady-state operating point exists and the corresponding small-signal model is stable, the operating point is considered to be stable.

Using the method described above, the stability of the estimation-error dynamics with erroneous model parameters was analyzed for different values of the design parameters b and c. Fig. 2(a) shows the stability map in the design-parameter space for the parameter uncertainties of 20% and 40% in medium-speed operation. In the figure, the vertical axis is scaled with the inverse rotor speed in order to help the comparison of different speeds. The operating point in Fig. 2(a) is defined by $\hat{\omega}_{\mathrm{m}} = 0.5$ p.u., $i_{\mathrm{d}} = 0$, and $i_{\mathrm{q}} = 0.9$ p.u., where the current components are defined in estimated

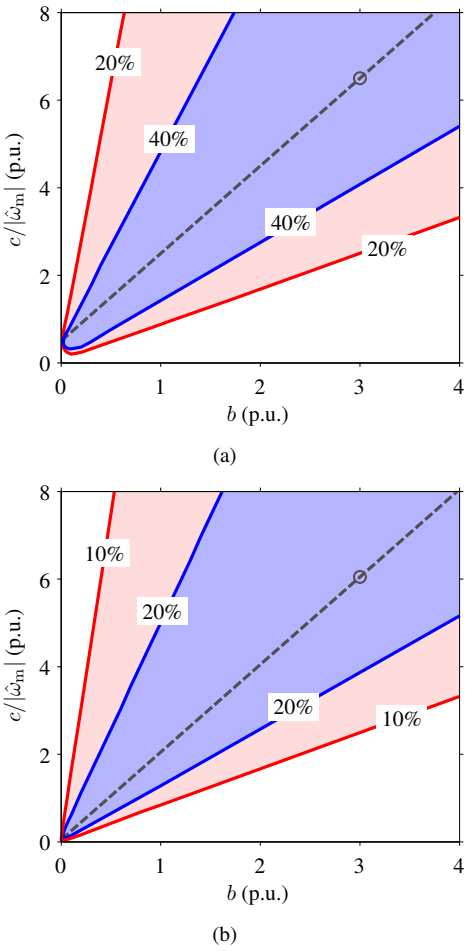

Fig. 2. Stability maps in the design parameter space. All $b > 0$ and $c > 0$ guarantee stable operation for accurate model parameters. (a) The operating point corresponds to $\hat{\omega}_\mathrm{m} = 0.5$ p.u., $i_\mathrm{d} = 0$, and $i_\mathrm{q} = 0.9$ p.u. The worst-case stability boundaries corresponding to the parameter uncertainties of 20% and 40% are shown by solid lines. (b) The operating point corresponds to $\hat{\omega}_\mathrm{m} = 0.05$ p.u., $i_\mathrm{d} = 0$, $i_\mathrm{q} = -0.9$ p.u. The worst-case stability boundaries corresponding to the parameter uncertainties of 10% and 20% are shown by solid lines. The dashed lines show (15) with $\kappa = 2$ and the circles correspond to the selection $b = 3$ p.u. (which is applied in the experiments).

rotor coordinates. The torque estimate corresponds to the rated motoring torque. It can be seen that the region of b and c yielding the stable operation is large even in the case of the parameter uncertainty of 40%.

Fig. 2(b) shows the stability map for parameter uncertainties of 10% and 20% in low-speed operation. The operating point is defined by $\hat{\omega}_\mathrm{m} = 0.05$ p.u., $i_\mathrm{d} = 0$ and $i_\mathrm{q} = -0.9$ p.u., i.e. the torque estimate corresponds to the rated generating torque. It can be seen that the shape of the regions is similar to Fig. 2(a) even if the speed is much lower and the torque is reversed. The stable regions would increase if the absolute torque were smaller (and they would shrink if the absolute torque were larger) while the shape of the regions remains similar.

The dashed lines in Fig. 2 correspond to

$$c = \kappa b|\hat{\omega}_\mathrm{m}| + \hat{\omega}_\mathrm{m}^2 \tag{15}$$

where the slope of the line is $\kappa = 2$. It can be seen that the lines in Fig. 2 pass approximately through the centers of the stable regions. Similar analysis was carried out in several other operating points, and it was found out that the value of κ can be kept constant. Hence, from the point of view of the robustness, it seems reasonable to fix the ratio of b and c according to (15), yielding the gains

$$k_1 = -b\frac{1 + \beta\kappa\,\mathrm{sign}(\hat{\omega}_\mathrm{m})}{\beta^2 + 1}, \quad k_2 = b\frac{\beta - \kappa\,\mathrm{sign}(\omega_\mathrm{m})}{\beta^2 + 1} \tag{16}$$

These gains are independent of the rotor speed estimate (except for its sign). Similar gains were applied in a preliminary study [31], but $\kappa = 1$ was fixed for simplicity, indicating a less robust design.

5) Stator-Resistance Adaptation: At low speeds, the accuracy of the model permanent-magnet flux has a comparatively small influence on the robustness. The effects of the magnetic saturation on the inductances can be taken into account in the model inductances.[4] The temperature-dependent stator resistance, however, is difficult to model. The robustness at low speeds can be improved by augmenting the observer with a stator-resistance adaptation law.

As already mentioned, an accurate model stator resistance $\hat{R}_\mathrm{s}$ was assumed in the derivation of (13), but this assumption will be lifted here. The following stator-resistance adaptation law is proposed:

$$\frac{\mathrm{d}\hat{R}_\mathrm{s}}{\mathrm{d}t} = k_\mathrm{R}(\hat{\psi}_\mathrm{d} - \hat{\psi}_\mathrm{pm} - \hat{L}_\mathrm{d} i_\mathrm{d}) \tag{17}$$

where k_R is the adaptation gain. As shown in Appendix B, the general stability conditions for the observer augmented with (17) are

$$k_\mathrm{R}(i_\mathrm{q} + \beta i_\mathrm{d})\hat{\omega}_\mathrm{m} > 0 \tag{18a}$$

$$k_\mathrm{R}[(i_\mathrm{d} - \beta i_\mathrm{q})b - (i_\mathrm{q} + \beta i_\mathrm{d})\hat{\omega}_\mathrm{m}] + bc > 0 \tag{18b}$$

where b and c are the positive design parameters in (13).

The stability conditions will be applied in the following. Based on the condition (18a), the sign of the gain k_R has to depend on the operating mode. Furthermore, the magnitude of k_R has to be limited according to (18b). It can be shown that the conditions in (18) are fulfilled by choosing

$$k_\mathrm{R} = \begin{cases} \min\{k'_\mathrm{R}, L\}, & \text{if } x > 0 \text{ and } L > 0 \\ \max\{-k'_\mathrm{R}, L\}, & \text{if } x < 0 \text{ and } L < 0 \\ k'_\mathrm{R}\,\mathrm{sign}(x), & \text{otherwise} \end{cases} \tag{19}$$

where k'_R is a positive design parameter. The sign of the gain k_R is determined by $x = (i_\mathrm{q} + \beta i_\mathrm{d})\hat{\omega}_\mathrm{m}$. The limiting value is

$$L = -r\frac{bc}{(i_\mathrm{d} - \beta i_\mathrm{q})b - (i_\mathrm{q} + \beta i_\mathrm{d})\hat{\omega}_\mathrm{m}} \tag{20}$$

where the parameter $0 < r < 1$ affects the stability margin of the system; choosing $r = 1$ would lead to a marginally stable system (in the operating points where k_R is determined by L).

In practice, the adaptation should be disabled in the vicinity of no-load operation and at higher stator frequencies due to poor signal-to-noise ratio (which is a fundamental property common to all stator-resistance adaptation methods based only

[4]Constant model inductances were used in this paper.

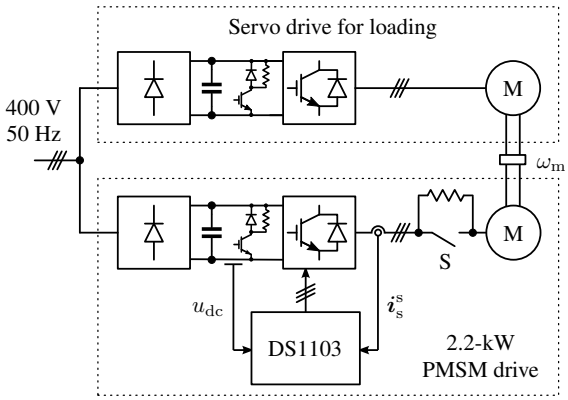

Fig. 3. Experimental setup. The stator currents and the dc-link voltage are used as feedback signals. Mechanical load is provided by a servo drive. The rotor speed $\omega_{\rm m}$ is measured for monitoring purposes. Three-phase switch S is in the closed position, except in the experiment shown in Fig. 6.

on the fundamental-wave excitation). Hence, parameter $k'_{\rm R}$ in (19) can be selected as

$$k'_{\rm R} = \begin{cases} k''_{\rm R}\left(1 - \frac{|\hat{\omega}_{\rm m}|}{\omega_\Delta}\right) i_{\rm s}, & \text{if } i_{\rm s} > i_\Delta \text{ and } |\hat{\omega}_{\rm m}| < \omega_\Delta \\ 0, & \text{otherwise} \end{cases} \tag{21}$$

where $k''_{\rm R}$, ω_Δ, and i_Δ are positive constants, and $i_{\rm s}$ is the magnitude of the stator-current vector.

IV. Experimental Results

A. Experimental Setup and Parameters

The operation of the proposed observer and stator-resistance adaptation was investigated experimentally using the setup shown in Fig. 3. The motion-sensorless control system was implemented in a dSPACE DS1103 PPC/DSP board. A 2.2-kW six-pole salient PMSM is fed by a frequency converter that is controlled by the DS1103 board. The rated values and the parameters of the PMSM are given in Table I.

A servo PMSM is used as a loading machine. The rotor speed $\omega_{\rm m}$ and position $\vartheta_{\rm m}$ are measured using an incremental encoder for monitoring purposes. The total moment of inertia of the experimental setup is 0.015 kgm^2 (2.2 times the inertia of the 2.2-kW PMSM rotor).

The stator resistance of the 2.2-kW PMSM is approximately 3.3 Ω at room temperature. Additional 1-Ω resistors were added between the frequency converter and the PMSM. The resistance can be changed stepwise by opening or closing a manually operated three-phase switch (S) connected in parallel with the resistors. Unless otherwise noted, switch S is in the closed position.

The block diagram of the speed-sensorless control system implemented in the DS1103 board is shown in Fig. 1. For simplicity, the components of the current reference vector were evaluated as $i_{\rm d,ref} = 0$ and $i_{\rm q,ref} = T_{\rm e,ref}/\hat{\psi}_{\rm pm}$. The control system is augmented with a speed controller, whose feedback signal is the speed estimate $\hat{\omega}_{\rm m}$ obtained from the proposed observer. The bandwidth of this PI controller, including active damping [32], is 0.08 p.u. The estimate of the per-unit electromagnetic torque is evaluated as $\hat{T}_{\rm e} = \hat{\psi}_{\rm pm} i_{\rm q} + (\hat{L}_{\rm d} - \hat{L}_{\rm q}) i_{\rm d} i_{\rm q}$.

The phase currents are measured using LEM LA 55-P/SP1 transducers. The sampling is synchronized to the modulation, and both the switching frequency and the sampling frequency are 5 kHz (i.e., the sampling period $T_{\rm s} = 200$ μs). The dc-link voltage is measured, and the reference voltage obtained from the current controller is used for the observer. The effect of inverter nonlinearities on the stator voltage is substantial at low speeds. Therefore, the most significant inverter nonlinearities, i.e. the dead-time effect and power device voltage drops, have to be compensated for [33], [34]. Using phase a as an example, a compensated duty cycle was evaluated as [35]

$$d_{\rm a} = d_{\rm a,ref} + \frac{2d_\delta}{\pi} \arctan\left(\frac{i_{\rm a}}{i_\delta}\right) \tag{22}$$

where $d_{\rm a,ref}$ is the ideal duty cycle obtained from the current controller and $i_{\rm a}$ is the phase current. The parameter $d_\delta = 0.011$ p.u. takes into account both the dead-time effect and the threshold voltage of the power devices, while the on-state slope resistance of the power devices is included in the model stator resistance. The shape of the arctan function is determined by the parameter $i_\delta = 0.21$ p.u. The current-feedforward compensation method in (22) corresponds to the method in [33], [34], except that the signum functions were replaced with the arctan functions in order to improve the performance in the vicinity of current zero crossings.

The proposed observer was implemented in estimated rotor coordinates using (11), (16), (17), (19), and (21). The adaptation law (17) was discretized as $\hat{R}_{\rm s}^{k+1} = \hat{R}_{\rm s}^k + T_{\rm s} k_{\rm R} (\hat{\psi}_{\rm d}^k - \hat{\psi}_{\rm pm} - \hat{L}_{\rm d} i_{\rm d}^k)$. The per-unit model parameters used in the experiments are: $\hat{L}_{\rm d} = 0.35$ p.u.; $\hat{L}_{\rm q} = 0.53$ p.u.; and $\hat{\psi}_{\rm pm} = 0.895$ p.u. The observer gain (16) is determined by the constants $b = 3$ p.u. and $\kappa = 2$. The parameters needed for the stator-resistance adaptation are: $r = 0.1$ in (20) and $k''_{\rm R} = 0.02$ p.u., $\omega_\Delta = 0.25$ p.u., and $i_\Delta = 0.2$ p.u. in (21).

B. Results

Fig. 4 shows results of medium-speed no-load operation. The speed reference was stepped from 0 to 1200 rpm, then to −1200 rpm and finally back to 0. According to (21), the stator-resistance adaptation was only active in the beginning of the acceleration and at the end of the deceleration. Even though there is an initial error of approximately 14 electrical degrees in the rotor position estimate, it can be seen that the position estimate converges close to the actual position in the beginning of the acceleration. The position error increases slightly at the end of the deceleration ($t > 2.5$ s) since the stator current, voltage and frequency approach zero and, therefore, there is no information available on the position. However, it is worth noticing that the position estimate remains stable at zero speed and the drive could be accelerated again.

Fig. 5 shows the effect of parameter errors on the position estimation error at the speed of 750 rpm under the rated load torque. The data was captured by varying each model parameter slowly (in six seconds) from 60% up to 140% of the actual value. It can be seen that the system remains stable in accordance with Fig. 2(a). The model parameters $\hat{R}_{\rm s}$ and $\hat{L}_{\rm d}$ have marginal effect on the position error. The errors in $\hat{L}_{\rm q}$ and $\hat{\psi}_{\rm pm}$ cause position error while the stability is not affected.

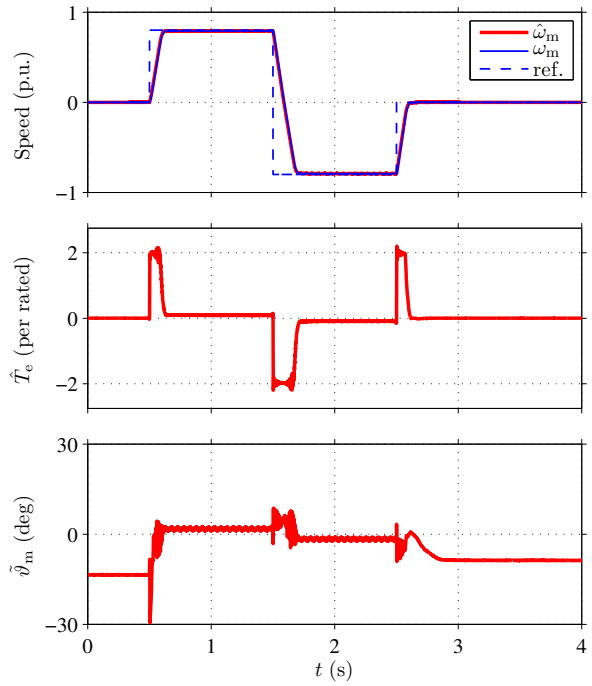

Fig. 4. Experimental results showing speed-reference steps (0 → 1200 rpm → −1200 rpm → 0) at no load.

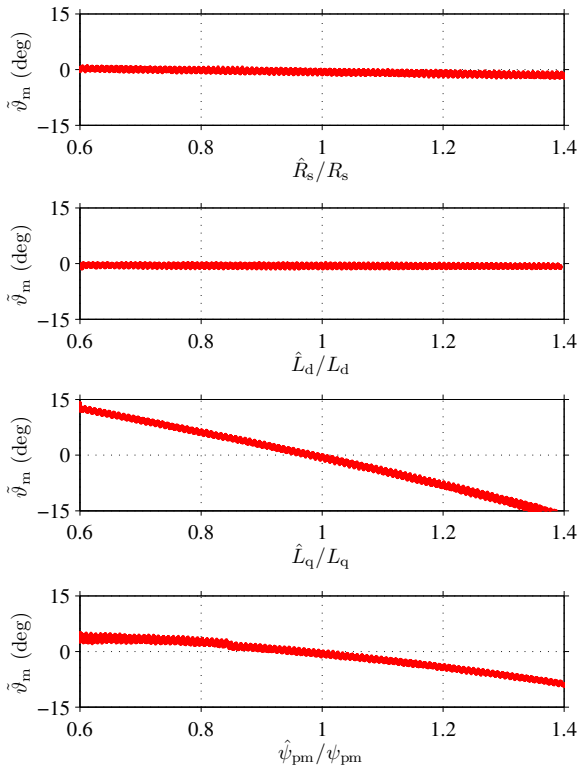

Fig. 5. Measured steady-state errors in the position estimate at the speed of 750 rpm under rated load torque. The data is captured by varying each model parameter slowly (in six seconds) from 60% up to 140% of the actual value.

Fig. 6 shows the stepwise change in the stator resistance (as seen by the frequency converter). Initially, three-phase switch S, cf. Fig. 3, was in the closed position. The speed reference was kept at 45 rpm. A rated-load torque step was applied at $t = 2$ s. Switch S was opened at $t = 5$ s, causing a 0.02-p.u. increase (corresponding to 30%) in the actual stator resistance. Switch S was closed at $t = 15$ s. It can be seen that the stator-resistance estimate tracks the change in the actual stator resistance.

Fig. 7 shows load-torque steps when the speed reference was kept at 30 rpm. The load torque was stepped to the rated value at $t = 1$ s, reversed at $t = 3$ s, and removed at $t = 5$ s. It can be seen that the proposed observer behaves well in torque transients. The ripple appearing in the measured waveforms originates mainly from the spatial flux and inductance harmonics that are comparatively strong in the studied PMSM [36]. They were not compensated in this study.

Results of slow speed reversals are shown in Fig. 8. A rated-load torque step was applied at $t = 2$ s. The speed reference was slowly ramped from 150 rpm to −150 rpm and back to 150 rpm. During the sequence, the drive operates in the motoring and regenerating modes. In the vicinity of zero frequency, the rotor-position estimate begins to deviate from the actual position but the system remains stable. Without the stabilizing observer gain, this kind of speed reversals would not be possible. Furthermore, without the stator-resistance adaptation, a very accurate model stator resistance would be needed since the frequency remains in the vicinity of zero for a long time.

V. Conclusions

In this paper, a reduced-order position observer with stator-resistance adaptation was proposed for motion-sensorless PMSM drives. A general analytical solution for the stabilizing observer gain and stability conditions for the stator-resistance adaptation were derived. Under these conditions, the local stability of the position and stator-resistance estimation is guaranteed at every operating point except the zero frequency, if other motor parameters are known. In the parametrization of the observer gains, sensitivity to the erroneous model parameters was taken into account. The proposed observer design is simple, and it results in a comparatively robust and well-damped closed-loop system. The observer was experimentally tested using a 2.2-kW PMSM drive; stable operation at low speeds under different loading conditions is demonstrated. Furthermore, it was experimentally verified that the stator-resistance estimate can track stepwise changes in the actual resistance.

Appendix A
Derivation of a Stabilizing Observer Gain

The local stability of the system (12) can be studied via small-signal linearization in the synchronous coordinates. Accurate model parameters $\hat{R}_\mathrm{s}$, $\hat{L}_\mathrm{d}$, $\hat{L}_\mathrm{q}$, and $\hat{\psi}_\mathrm{pm}$ are assumed

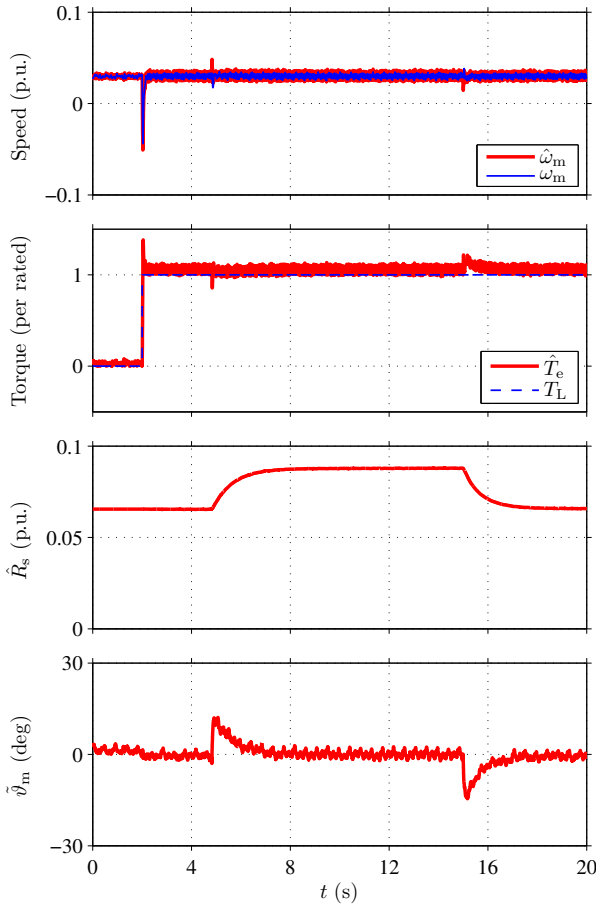

Fig. 6. Experimental results showing the stepwise increase of 1 Ω in the actual stator resistance at $t = 5$ s and the decrease at $t = 15$ s. Speed reference is kept at 45 rpm and rated load torque is applied at $t = 2$ s. T_L shown in the second subplot is the torque reference of the loading drive.

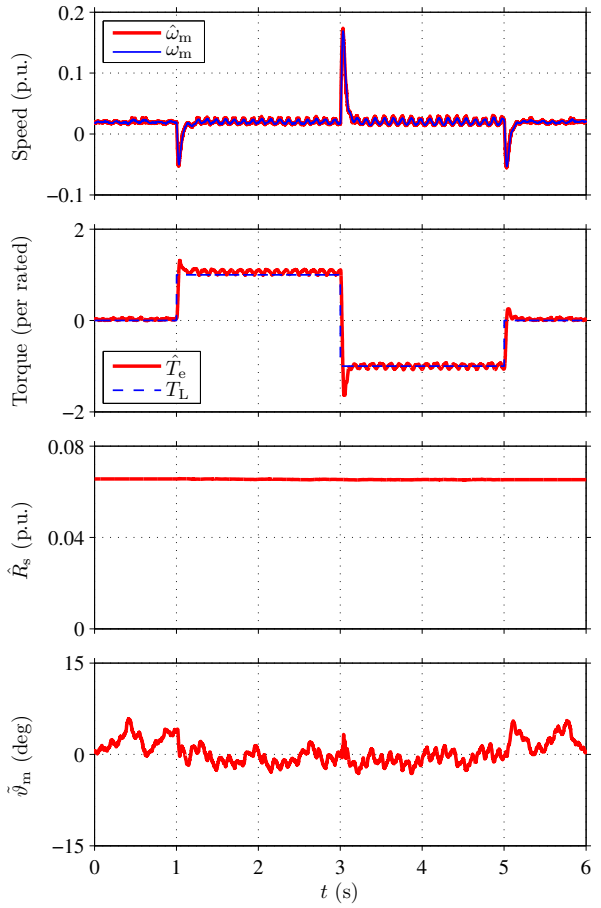

Fig. 7. Experimental results showing load-torque steps (0 → rated → negative rated → 0) when the speed reference is kept at 30 rpm.

in the following. When the definition (8) and the observer gain (9) are applied in (12), linearization results in

$$\frac{\mathrm{d}}{\mathrm{d}t}\begin{bmatrix}\tilde{\psi}_\mathrm{d}\\ \tilde{\psi}_\mathrm{q}\end{bmatrix} = \underbrace{\begin{bmatrix}k_{10} & -k_{10}\beta_0+\omega_{\mathrm{m}0}\\ k_{20}-\omega_{\mathrm{m}0} & -k_{20}\beta_0\end{bmatrix}}_{\boldsymbol{A}}\begin{bmatrix}\tilde{\psi}_\mathrm{d}\\ \tilde{\psi}_\mathrm{q}\end{bmatrix} \tag{23}$$

where the operating-point quantities are marked by the subscript 0. It is worth noticing that $\tilde{\vartheta}_\mathrm{m}$ and $\tilde{\psi}_\mathrm{q}$ of the linearized system are linearly dependent, i.e. $\tilde{\psi}_\mathrm{q} = [\psi_\mathrm{pm} + (L_\mathrm{d} - L_\mathrm{q})i_{\mathrm{d}0}]\tilde{\vartheta}_\mathrm{m}$ holds.

Since accurate model parameters are assumed, $\tilde{\psi}_{\mathrm{d}0} = 0$ and $\tilde{\vartheta}_{\mathrm{m}0} = 0$ hold in the operating point. Therefore, the linearization is valid even if the gain scheduling is used for the observer gain. The characteristic polynomial is $\det(s\mathbf{I}-\boldsymbol{A}) = s^2 + b_0 s + c_0$, where

$$b_0 = k_{20}\beta_0 - k_{10}, \quad c_0 = \omega_{\mathrm{m}0}^2 - (k_{20} + k_{10}\beta_0)\omega_{\mathrm{m}0} \tag{24}$$

The nonlinear system (12) is locally stable if the coefficients of the characteristic polynomial are positive: $b_0 > 0$ and $c_0 > 0$.

From (24), the general stabilizing gain can be solved:

$$k_{10} = -\frac{b_0 + \beta_0(c_0/\omega_{\mathrm{m}0} - \omega_{\mathrm{m}0})}{\beta_0^2 + 1} \tag{25a}$$

$$k_{20} = \frac{\beta_0 b_0 - c_0/\omega_{\mathrm{m}0} + \omega_{\mathrm{m}0}}{\beta_0^2 + 1} \tag{25b}$$

This gain is related to the closed-loop poles according to

$$s_{1,2} = \frac{-b_0 \pm \sqrt{b_0^2 - 4c_0}}{2}. \tag{26}$$

and to the damping ratio and undamped natural frequency according to

$$\zeta = \frac{b_0}{2\sqrt{c_0}}, \quad \omega_\mathrm{n} = \sqrt{c_0} \tag{27}$$

respectively.

Appendix B
Stability of Stator-Resistance Adaptation

Accurate model parameters $\hat{L}_\mathrm{d}$, $\hat{L}_\mathrm{q}$, and $\hat{\psi}_\mathrm{pm}$ are assumed in the following. Assuming constant actual resistance R_s and the stator-resistance adaptation law (17), the nonlinear dynamics of the stator-resistance estimation error become

$$\frac{\mathrm{d}\tilde{R}_\mathrm{s}}{\mathrm{d}t} = k_\mathrm{R}(\hat{\psi}_\mathrm{d} - \psi_\mathrm{pm} - L_\mathrm{d} i_\mathrm{d}) \tag{28}$$

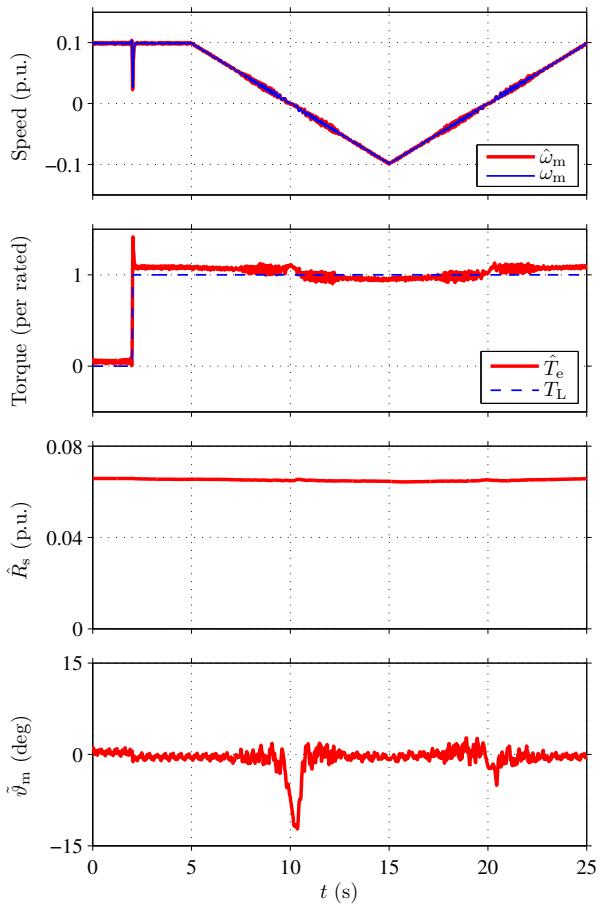

Fig. 8. Experimental results showing slow speed reversals (150 rpm $\rightarrow -150$ rpm $\rightarrow$ 150 rpm) when the rated load torque is applied.

The closed-loop system consisting of (12) and (28) can be linearized:

$$\frac{\mathrm{d}}{\mathrm{d}t}\begin{bmatrix}\tilde{\psi}_\mathrm{d}\\ \tilde{\psi}_\mathrm{q}\\ \tilde{R}_\mathrm{s}\end{bmatrix} = \begin{bmatrix}k_{10} & -k_{10}\beta_0+\omega_{\mathrm{m}0} & -i_{\mathrm{d}0}\\ k_{20}-\omega_{\mathrm{m}0} & -k_{20}\beta_0 & -i_{\mathrm{q}0}\\ k_{\mathrm{R}0} & -k_{\mathrm{R}0}\beta_0 & 0\end{bmatrix}\begin{bmatrix}\tilde{\psi}_\mathrm{d}\\ \tilde{\psi}_\mathrm{q}\\ \tilde{R}_\mathrm{s}\end{bmatrix} \quad (29)$$

where the definition (8) and the observer gain (9) are applied. Using the Routh–Hurwitz stability criterion, the stability conditions are

$$b_0 > 0 \quad (30a)$$

$$k_{\mathrm{R}0}(i_{\mathrm{q}0} + \beta_0 i_{\mathrm{d}0})\omega_{\mathrm{m}0} > 0 \quad (30b)$$

$$k_{\mathrm{R}0}[(i_{\mathrm{d}0} - \beta_0 i_{\mathrm{q}0})b_0 - (i_{\mathrm{q}0} + \beta i_{\mathrm{d}0})\omega_{\mathrm{m}0}] + b_0 c_0 > 0 \quad (30c)$$

Acknowledgment

The authors gratefully acknowledge the Academy of Finland and ABB Oy for the financial support.

References

[1] P. L. Jansen and R. D. Lorenz, "Transducerless position and velocity estimation in induction and salient AC machines," *IEEE Trans. Ind. Appl.*, vol. 31, no. 2, pp. 240–247, Mar./Apr. 1995.

[2] M. Schroedl, "Sensorless control of AC machines at low speed and standstill based on the "INFORM" method," in *Conf. Rec. IEEE-IAS Annu. Meeting*, vol. 2, San Diego, CA, Oct. 1996, pp. 270–277.

[3] J. Holtz, "Acquisition of position error and magnet polarity for sensorless control of PM synchronous machines," *IEEE Trans. Ind. Appl.*, vol. 44, no. 4, pp. 1172–1180, July/Aug. 2008.

[4] P. Guglielmi, M. Pastorelli, G. Pellegrino, and A. Vagati, "Position-sensorless control of permanent-magnet-assisted synchronous reluctance motor," *IEEE Trans. Ind. Appl.*, vol. 40, no. 2, pp. 615–622, Mar./Apr. 2004.

[5] A. Piippo, M. Hinkkanen, and J. Luomi, "Sensorless control of PMSM drives using a combination of voltage model and HF signal injection," in *Conf. Rec. IEEE-IAS Annu. Meeting*, vol. 2, Seattle, WA, Oct. 2004, pp. 964–970.

[6] O. Wallmark, L. Harnefors, and O. Carlson, "An improved speed and position estimator for salient permanent-magnet synchronous motors," *IEEE Trans. Ind. Electron.*, vol. 52, no. 1, pp. 255–262, Feb. 2005.

[7] C. Silva, G. M. Asher, and M. Sumner, "Hybrid rotor position observer for wide speed-range sensorless PM motor drives including zero speed," *IEEE Trans. Ind. Electron.*, vol. 53, no. 2, pp. 373–378, Apr. 2006.

[8] A. Piippo, M. Hinkkanen, and J. Luomi, "Analysis of an adaptive observer for sensorless control of interior permanent magnet synchronous motors," *IEEE Trans. Ind. Electron.*, vol. 55, no. 2, pp. 570–576, Feb. 2008.

[9] W. Hammel and R. M. Kennel, "Position sensorless control of PMSM by synchronous injection and demodulation of alternating carrier voltage," in *Proc. IEEE SLED 2010*, Padova, Italy, July 2010, pp. 56–63.

[10] L. Harnefors and H.-P. Nee, "A general algorithm for speed and position estimation of AC motors," *IEEE Trans. Ind. Electron.*, vol. 47, no. 1, pp. 77–83, Feb. 2000.

[11] M. Jansson, L. Harnefors, O. Wallmark, and M. Leksell, "Synchronization at startup and stable rotation reversal of sensorless nonsalient PMSM drives," *IEEE Trans. Ind. Electron.*, vol. 53, no. 2, pp. 379–387, Apr. 2006.

[12] I. Boldea, M. C. Paicu, G.-D. Andreescu, and F. Blaabjerg, ""Active flux" DTFC-SVM sensorless control of IPMSM," *IEEE Trans. Energy Convers.*, vol. 24, no. 2, pp. 314–322, June 2009.

[13] R. Wu and G. R. Slemon, "A permanent magnet motor drive without a shaft sensor," *IEEE Trans. Ind. Appl.*, vol. 27, no. 5, pp. 1005–1011, Sep./Oct. 1991.

[14] R. Dhaouadi, N. Mohan, and L. Norum, "Design and implementation of an extended kalman filter for the state estimation of a permanent magnet synchronous motor," *IEEE Trans. Power Electron.*, vol. 6, no. 3, pp. 491–497, July 1991.

[15] N. Matsui and M. Shigyo, "Brushless dc motor control without position and speed sensors," *IEEE Trans. Ind. Appl.*, vol. 28, no. 1, pp. 120–127, Jan./Feb. 1992.

[16] G. Yang, R. Tomioka, M. Nakano, and T. H. Chin, "Position and speed sensorless control of brushless DC motor based on an adaptive observer," *IEEJ Trans. Ind. Appl.*, vol. 113, pp. 579–586, May 1993.

[17] A. Consoli, S. Musumeci, A. Raciti, and A. Testa, "Sensorless vector and speed control of brushless motor drives," *IEEE Trans. Ind. Electron.*, vol. 41, no. 1, pp. 91–95, Feb. 1994.

[18] J.-S. Kim and S.-K. Sul, "High performance PMSM drives without rotational sensors using reduced order observer," in *Conf. Rec. IEEE-IAS Annu. Meeting*, vol. 1, Orlando, FL, Oct. 1995, pp. 75–82.

[19] K.-H. Kim, S.-K. Chung, G.-W. Moon, I.-C. Baik, and M.-J. Youn, "Parameter estimation and control for permanent magnet synchronous motor drive using model reference adaptive technique," in *Proc. IEEE IECON'95*, vol. 1, Orlando, FL, Nov. 1995, pp. 387–392.

[20] S. Bolognani, R. Oboe, and M. Zigliotto, "Sensorless full-digital PMSM drive with EKF estimation of speed and rotor position," *IEEE Trans. Ind. Electron.*, vol. 46, no. 1, pp. 184–191, Feb. 1999.

[21] Y.-S. Han, J.-S. Choi, and Y.-S. Kim, "Sensorless PMSM drive with a sliding mode control based adaptive speed and stator resistance estimator," vol. 36, no. 5, pp. 3588–3591, Sept. 2000.

[22] H. Kim, M. C. Harke, and R. D. Lorenz, "Sensorless control of interior permanent-magnet machine drives with zero-phase lag position estimation," *IEEE Trans. Ind. Appl.*, vol. 39, no. 6, pp. 1726–1733, Nov./Dec. 2003.

[23] B. Nahid-Mobarakeh, F. Meibody-Tabar, and F.-M. Sargos, "Mechanical sensorless control of PMSM with online estimation of stator resistance," *IEEE Trans. Ind. Appl.*, vol. 40, no. 2, pp. 457–471, Mar./Apr. 2004.

[24] S. Shinnaka, "New "D-state-observer"-based vector control for sensorless drive of permanent-magnet synchronous motors," *IEEE Trans. Ind. Appl.*, vol. 41, no. 3, pp. 825–833, May/June 2005.

[25] S. Koonlaboon and S. Sangwongwanich, "Sensorless control of interior permanent-magnet synchronous motors based on a fictitious permanent-magnet flux model," in *Conf. Rec. IEEE-IAS Annu. Meeting*, Hong Kong, Oct. 2005, pp. 311–318.

[26] S. Morimoto, M. Sanada, and Y. Takeda, "Mechanical sensorless drives of IPMSM with online parameter identification," *IEEE Trans. Ind. Appl.*, vol. 42, no. 5, pp. 1241–1248, Sep./Oct. 2006.

[27] S. Ichikawa, M. Tomita, S. Doki, and S. Okuma, "Sensorless control of permanent-magnet synchronous motors using online parameter identification based on system identification theory," *IEEE Trans. Ind. Electron.*, vol. 53, no. 2, pp. 363–372, Apr. 2006.

[28] E. Urlep and K. Jezernik, "Low and zero speed sensorless control of nonsalient PMSM," in *Proc. IEEE ISIE'07*, Vigo, Spain, June 2007, pp. 2238–2243, CD-ROM.

[29] S. Sangwongwanich, S. Suwankawin, S. Po-ngam, and S. Koonlaboon, "A unified speed estimation design framework for sensorless ac motor drives based on positive-real property," in *Proc. PCC-Nagoya'07*, Nagoya, Japan, Apr. 2007, pp. 1111–1118.

[30] J. Lee, J. Hong, K. Nam, R. Ortega, L. Praly, and A. Astolfi, "Sensorless control of surface-mount permanent-magnet synchronous motors based on a nonlinear observer," *IEEE Trans. Power Electron.*, vol. 25, no. 2, pp. 290–297, Feb. 2010.

[31] M. Hinkkanen, T. Tuovinen, L. Harnefors, and J. Luomi, "A reduced-order position observer with stator-resistance adaptation for PMSM drives," in *Proc. IEEE ISIE'10*, Bari, Italy, July 2010, pp. 3071–3076.

[32] L. Harnefors, "Design and analysis of general rotor-flux-oriented vector control systems," *IEEE Trans. Ind. Electron.*, vol. 48, no. 2, pp. 383–390, Apr. 2001.

[33] J. K. Pedersen, F. Blaabjerg, J. W. Jensen, and P. Thogersen, "An ideal PWM-VSI inverter with feedforward and feedback compensation," in *Proc. EPE'93*, vol. 4, Brighton, U.K., Sept. 1993, pp. 312–318.

[34] J.-W. Choi and S.-K. Sul, "Inverter output voltage synthesis using novel dead time compensation," *IEEE Trans. Power Electron.*, vol. 11, no. 2, pp. 221–227, Mar. 1996.

[35] M. Hinkkanen, L. Harnefors, and J. Luomi, "Reduced-order flux observers with stator-resistance adaptation for speed-sensorless induction motor drives," *IEEE Trans. Power Electron.*, vol. 25, no. 5, pp. 1173–1183, May 2010.

[36] A. Piippo and J. Luomi, "Torque ripple reduction in sensorless PMSM drives," in *Proc. IEEE IECON'06*, Paris, France, Nov. 2006, pp. 920–925.

Marko Hinkkanen (M'06) received the M.Sc.(Eng.) and D.Sc.(Tech.) degrees from the Helsinki University of Technology, Espoo, Finland, in 2000 and 2004, respectively.

Since 2000, he has been with the Helsinki University of Technology (part of Aalto University since 2010). He is currently an Adjunct Professor in the Aalto University School of Electrical Engineering, Espoo, Finland. His research interests include electric drives and electric machines.

Toni Tuovinen received the M.Sc. degree from the University of Helsinki, Helsinki, Finland, in 2005, and the M.Sc.(Eng.) degree from Helsinki University of Technology, Espoo, Finland, in 2009.

Since 2007, he has been with the Helsinki University of Technology (part of Aalto University since 2010). He is currently a Research Scientist in the Aalto University School of Electrical Engineering, Espoo, Finland. His main research interest is the control of electric drives.

Lennart Harnefors (S'93–M'97–SM'08) was born in 1968 in Eskilstuna, Sweden. He received the M.Sc., Licentiate, and Ph.D. degrees in electrical engineering from the Royal Institute of Technology, Stockholm, Sweden, and the Docent (D.Sc.) degree in industrial automation from Lund University, Lund, Sweden, in 1993, 1995, 1997, and 2000, respectively.

From 1994 to 2005, he was with Mälardalen University, Västerås, Sweden, where he, in 2001, was appointed as a Professor of electrical engineering. From 2001 to 2006, he was also a part-time Visiting Professor of electrical drives with Chalmers University of Technology, Göteborg, Sweden. He is currently an R&D Project Manager with ABB, Power Systems - HVDC, Ludvika, Sweden and an Adjunct Professor of power electronics with the Royal Institute of Technology, Stockholm, Sweden. His research interests include grid-connected converters and ac drives.

Dr. Harnefors is an Associate Editor of the IEEE TRANSACTIONS ON INDUSTRIAL ELECTRONICS and the *International Journal of Power Electronics*. He was the recipient of the 2000 ABB Gunnar Engström Energy Award and the 2002 IEEE TRANSACTIONS ON INDUSTRIAL ELECTRONICS Best Paper Award.

Jorma Luomi (M'92) received the M.Sc.(Eng.) and D.Sc.(Tech.) degrees from the Helsinki University of Technology, Espoo, Finland, in 1977 and 1984, respectively.

He joined the Helsinki University of Technology in 1980, and from 1991 to 1998, he was a Professor at Chalmers University of Technology, Göteborg, Sweden. He is currently a Professor in the Aalto University School of Electrical Engineering, Espoo, Finland. His research interests include electric drives, electric machines, and numerical analysis of electromagnetic fields.